

PROGRESS IN INORGANIC CHEMISTRY

An Appreciation of Henry Taube

Edited by

STEPHEN J. LIPPARD

DEPARTMENT OF CHEMISTRY
MASSACHUSETTS INSTITUTE OF TECHNOLOGY
CAMBRIDGE, MASSACHUSETTS

VOLUME 30

AN INTERSCIENCE® PUBLICATION

JOHN WILEY & SONS

New York • Chichester • Brisbane • Toronto • Singapore

***Progress in
Inorganic Chemistry***

Volume 30

Advisory Board

THEODORE L. BROWN

UNIVERSITY OF ILLINOIS, URBANA, ILLINOIS

JAMES P. COLLMAN

STANFORD UNIVERSITY, STANFORD, CALIFORNIA

F. ALBERT COTTON

TEXAS A & M UNIVERSITY, COLLEGE STATION, TEXAS

RONALD J. GILLESPIE

McMASTER UNIVERSITY, HAMILTON, ONTARIO, CANADA

RICHARD H. HOLM

HARVARD UNIVERSITY, CAMBRIDGE, MASSACHUSETTS

GEOFFREY WILKINSON

IMPERIAL COLLEGE OF SCIENCE AND TECHNOLOGY, LONDON,
ENGLAND

PROGRESS IN INORGANIC CHEMISTRY

An Appreciation of Henry Taube

Edited by

STEPHEN J. LIPPARD

DEPARTMENT OF CHEMISTRY
MASSACHUSETTS INSTITUTE OF TECHNOLOGY
CAMBRIDGE, MASSACHUSETTS

VOLUME 30

AN INTERSCIENCE® PUBLICATION

JOHN WILEY & SONS

New York • Chichester • Brisbane • Toronto • Singapore

An Interscience® Publication

Copyright © 1983 by John Wiley & Sons, Inc.

All rights reserved. Published simultaneously in Canada.

Reproduction or translation of any part of this work beyond that permitted by Section 107 or 108 of the 1976 United States Copyright Act without the permission of the copyright owner is unlawful. Requests for permission or further information should be addressed to the Permissions Department, John Wiley & Sons, Inc.

Library of Congress Cataloging in Publication Data:

Main entry under title:

Progress in inorganic chemistry.

(Progress in inorganic chemistry; v. 30)

"An Interscience publication."

Includes indexes.

I. Chemistry, Inorganic—Addresses, essays, lectures.

I. Taube, Henry, 1915- II. Lippard, Stephen J.

III. Series.

QD151.P76 vol. 30 [QD152] 546s [546] 82-20111

ISBN 0-471-87022-6

Printed in the United States of America

10 9 8 7 6 5 4 3 2 1

Foreword

Henry Taube and his research accomplishments are held in universally high esteem, and this foreword provides an opportunity to recall the basis for the universal acclaim. Looking at his work as a whole, we see that Taube has made a major contribution in helping to develop a systematic basis for the understanding of the dynamic behavior of inorganic compounds, both of the transition metals and of the representative elements, and his work has played an important role in helping to create a modern renaissance in inorganic chemistry. In addition, he has developed both experimental methods and mechanistic concepts that have had a lasting impact in all areas of chemistry.

It is revealing to consider some of his specific contributions both for their immediate impact and for the foundations they laid for further research.

Taube's work provided the first determination of the hydration numbers of aqueous metal cations and the first applications of a number of experimental techniques to this problem, including oxygen isotopic labelling, NMR chemical shift measurements, and NMR paramagnetic shifts. Taube was the first to measure the equilibrium between inner and outer sphere forms of complex ions, which helped set the stage for detailed mechanistic studies in solution. In his classic review article of 1952, he pointed to the correlations that exist between ligand substitution rates and the electronic configuration at the metal, an observation that continues to provide an important theoretical basis for our understanding of substitution reactions. Experimentally, his work in substitution chemistry was noted for its originality and for the experimental foundation that it provided for subsequent mechanistic studies. For example, he was the first to demonstrate the rate law for substitution in square planar complexes and to show how pressure effects could be used to diagnose substitution reactions involving metal complexes. From his work came the first applications of the product competition method as a technique for exploring substitution mechanisms. He also discovered and began the elucidation of the oxidative-substitution reaction.

Taube is perhaps most widely recognized for his pioneering work on the mechanism of oxidation-reduction reactions. In 1952, he first demonstrated the oxygen atom transfer pathway for a redox reaction in solution using isotopic tracer techniques. Shortly thereafter, he demonstrated the existence of the *inner-sphere* pathway for electron transfer between transition metal

complexes in an elegant experiment that took advantage of his earlier understanding of ligand exchange rates. In later experiments he was able to demonstrate that electron transfer could occur by *remote attack* where the reductant and oxidant occupy different binding sites on the bridging ligand. This work was followed by the elegant, rational design of a series of systems in which intramolecular electron transfer between metal ions through a bridging ligand could be measured directly.

Taube's group was the first to systematically prepare and characterize a series of discrete mixed-valence molecules. His original work in this area was literally the beginning of a new and growing area in chemistry. His continuing efforts have led to the development of mixed-valence complexes that have been of value in the study of redox processes and of electronic delocalization between chemical sites. An additional and continuing theme in Taube's recent work has been an effort to understand and exploit metal-to-ligand backbonding effects in metal complexes. As an early part of this effort, his group prepared the first bridging dinitrogen complex, first demonstrated the direct formation of a dinitrogen complex by reaction of a metal ion with dinitrogen in aqueous solution, and prepared the first *bis*-dinitrogen complex. His work on backbonding in classical coordination complexes represents the most definitive and wide-ranging experimental attack on this important electronic effect. Among the results derived from the work are a basis for understanding how the physical and chemical properties of a chemical complex can be altered systematically as a result of changing backbonding effects.

Taube's work is one of the keystones for our understanding of inorganic chemical reactivity. His work has transformed inorganic chemistry in a way matched by few other scientists since the time of Alfred Werner. Hopefully, a measure of this impact has been caught in the various accounts in the current volume of *Progress in Inorganic Chemistry*. The contributions which appear here certainly suggest something of the breadth of Taube's interests and of the significance of his impact on a wide range of subjects. Chapter topics vary from mixed-valence compounds by Carol Creutz to three chapters on different aspects of photochemistry by John Endicott et al., Peter Ford et al., and myself. There is a chapter on the descriptive chemistry of technetium by Edward Deutsch et al. and a chapter on applications of NMR to aquo complexes by John Hunt and Harold Friedman. Electron transfer is well represented by chapters on theory by Norman Sutin, electron transfer mechanisms by Albert Haim, and the role of electron transfer on metal-carbon bond homolysis by James Espenson.

I know that the authors of the various chapters have approached their tasks with enthusiasm and that they will join me in dedicating this volume to Henry Taube, an extraordinary scientist and at the same time an extraordinary man.

THOMAS J. MEYER

February 1983

Preface

The influence of Henry Taube on inorganic chemistry is profound. In appreciation of his contributions the Advisory Board and I decided to devote Volume 30 of *Progress in Inorganic Chemistry* to reviews summarizing the most recent developments in electron transfer reactions, mixed valence complexes, aquo complexes of metal ions, photosubstitution processes, and other topics inspired by the Taube school of thought. In this manner we celebrate not only 30 volumes of this review series but also the work of one of the leaders of the renaissance of our field. As with any such undertaking, the final product is a measure of the inspiration and cooperation of the individual contributors. I would therefore like to thank all the authors for their prompt submission of manuscripts, Tom Meyer for invaluable assistance in identifying the contributors, Dick Holm for making the initial suggestion that we produce a "Taube Volume," and finally Henry Taube for his cooperation and support.

STEPHEN J. LIPPARD

February 1983

Contents

- Mixed Valence Complexes of d^5 - d^6 Metal Centers 1
By CAROL CREUTZ
*Department of Chemistry, Brookhaven National Laboratory
Upton, New York*
- Technetium Chemistry and Technetium Radiopharmaceuticals . . . 75
By EDWARD DEUTSCH, KAREN LIBSON, and SILVIA JURISSON
*Department of Chemistry, University of Cincinnati
Cincinnati, Ohio*
and
LEONARD F. LINDOY
*Department of Chemistry and Biochemistry
James Cook University
Queensland, Australia*
- Structural and Photochemical Probes of Electron Transfer Reactivity 141
By JOHN F. ENDICOTT, KRISHAN KUMAR, T. RAMASAMI,
and FRANCOIS P. ROTZINGER
*Department of Chemistry, Wayne State University
Detroit, Michigan*
- Homolytic and Free Radical Pathways in the Reactions of
Organochromium Complexes 189
By JAMES H. ESPENSON
*Ames Laboratory and Department of Chemistry
Iowa State University
Ames, Iowa*
- Mechanistic Aspects of the Photosubstitution and
Photoisomerization Reactions of d^6 Metal Complexes 213
By PETER C. FORD, DAVID WINK, and JOHN DIBENEDETTO
*Department of Chemistry, University of California
Santa Barbara, California*

Mechanisms of Electron Transfer Reactions: The Bridged Activated Complex	273
By ALBERT HAIM <i>Department of Chemistry, State University of New York Stony Brook, New York</i>	
Aquo Complexes of Metal Ions	359
By J. P. HUNT <i>Department of Chemistry, Washington State University Pullman, Washington</i> and H. L. FRIEDMAN <i>Department of Chemistry, State University of New York Stony Brook, New York</i>	
Excited-State Electron Transfer	389
By THOMAS J. MEYER <i>Department of Chemistry, University of North Carolina Chapel Hill, North Carolina</i>	
Theory of Electron Transfer Reactions: Insights and Hindsights . . .	441
By NORMAN SUTIN <i>Department of Chemistry, Brookhaven National Laboratory Upton, New York</i>	
Subject Index	499
Cumulative Index, Volumes 1-30	521

***Progress in
Inorganic Chemistry***

Volume 30

Mixed Valence Complexes of d^5-d^6 Metal Centers

CAROL CREUTZ

*Department of Chemistry
Brookhaven National Laboratory
Upton, New York*

CONTENTS

I. INTRODUCTION	2
II. MIXED-VALENCE COMPLEXES AND THE DYNAMICS OF ELECTRON TRANSFER REACTIONS	4
A. General Considerations	4
B. Classification of Mixed-Valence Complexes	7
C. Analysis of Intervalence Spectra	9
III. THE FRAGMENTS: PROPERTIES OF THE MONONUCLEAR SYSTEMS	12
IV. CLASSIFICATION OF MIXED-VALENCE COMPLEXES: CASE HISTORIES FOR $[\text{Ru}(\text{NH}_3)_3]_2\text{L}-\text{L}^{5+}$	19
A. Problems: The Creutz-Taube Ion, $\text{L}-\text{L} = \text{pyrazine}$	19
B. Success of the Hush Model, $\text{L}-\text{L} = 4,4'$ -bipyridine	23
C. Strong Delocalization: $\text{L}-\text{L} = \text{cyanogen}$	25
D. Other Systems	25
V. STABILITIES OF MIXED-VALENCE COMPLEXES	26
A. Practical Considerations	26
B. General Thermodynamic Comparisons	27
C. The Comproportionation Equilibrium: Class II Systems	28
D. The Comproportionation Equilibrium: Class III Systems	31
E. Trends with Bridging Group and Metal Center	31
VI. INTERVALLENCE SPECTRA AND ELECTRON TRANSFER BARRIERS	38
A. The Magnitude of the Electronic Coupling	39
B. The Solvent Barrier	47

C. The Inner-Shell Barrier	54
D. The Thermodynamic Barrier	56
E. Calculation of Thermal Electron Transfer Rates	62
Abbreviations	68
Acknowledgments	69
References	69

I. INTRODUCTION

Mixed-valence materials—materials that contain an element in more than one oxidation state—have attracted the interest of chemists for many years (1, 6, 101). The reason for this interest is illustrated by the familiar (but nonetheless wonderful) result obtained when colorless solutions of $\text{Fe}_{\text{aq}}^{2+}$ and $\text{Fe}(\text{CN})_6^{3-}$ (or $\text{Fe}_{\text{aq}}^{3+}$ and $\text{Fe}(\text{CN})_6^{4-}$) are mixed and yield the deep blue material, Prussian blue or Turnbull's blue (144). The color of the Fe^{III} [$\text{Fe}^{\text{II}}(\text{CN})_6^{4-}$] salt produced arises because visible light absorption induces electron transfer from Fe^{II} to Fe^{III} , a phenomenon possible only in the mixed-valence material where both oxidation states are present. In the broadest sense, the subject of mixed-valence chemistry embraces organic, as well as inorganic, materials and species in the gas, solution, and solid phases, including both molecular and macromolecular solids. They are of interest (6) on account of their structures, their conductivities, and their magnetic properties, in addition to their spectral properties mentioned above. The subject is thus a broad and important one, in addition to being a very old one.

The aspects of the subject of mixed-valence chemistry to be addressed in this article are, however, of rather recent vintage and limited, for the most part, to the properties of discrete molecular species in solution. The systematic study of such species began in 1967–1970 as a result of several parallel developments. In 1967 Allen and Hush (1) and Robin and Day (101) published articles in which the physical properties of mixed-valence materials were systematically reviewed, and Hush (52) provided a theoretical bridge between the physical properties of these materials and the subject of electron transfer reactions in solution. Of greatest interest to mechanistic inorganic chemists was the prediction that moderately coupled mixed-valence compounds should exhibit intervalence transfer (light-induced metal-to-metal charge transfer) absorption at an energy E_{op} simply related to the energetic barrier for thermal electron transfer ($\Delta G_{\text{th}}^{\ddagger}$) in the same material.

For symmetric species,

$$E_{op} = 4 \Delta G_{th}^* \quad (1)$$

the bandwidth at half-intensity $\Delta\bar{\nu}_{1/2}$ (in cm^{-1}) should be a function of the band maximum $\bar{\nu}_{max}$ (in cm^{-1}). For a transition of this origin

$$\Delta\bar{\nu}_{1/2} = [2310 \bar{\nu}_{max}]^{1/2} \text{cm}^{-1} \quad (2)$$

In addition, the band position should be a function of solvent through Eqs. 3-5, where n is the number of ligands per metal center.

$$E_{op} = E_{in} + E_{out} \quad (3)$$

$$E_{in} = n \left(\frac{2f_2 f_3}{f_2 + f_3} \right) (d_2^0 - d_3^0)^2 \quad (4)$$

$$E_{out} = e^2 \left(\frac{1}{2a_2} + \frac{1}{2a_3} - \frac{1}{r} \right) \left(\frac{1}{D_{op}} - \frac{1}{D_s} \right) \quad (5)$$

a_2 , a_3 and f_2 , f_3 are the metal-ligand bond lengths and force constants for the metal in oxidation states II and III, respectively, r is the separation between the metal centers, and D_{op} and D_s are the optical and static dielectric constants of the solvents. Furthermore, measurement of the band intensity permitted evaluation of the degree of electronic coupling between the metal centers through Eq. 6 (1, 52) where ϵ_{max} is the molar absorptivity ($M^{-1}\text{cm}^{-1}$) at

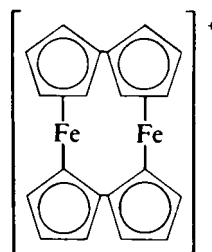
$$H_{AB} = 2.05 \times 10^{-2} \left[\frac{\epsilon_{max} \Delta\bar{\nu}_{1/2}}{\bar{\nu}_{max}} \right]^{1/2} \frac{\bar{\nu}_{max}}{r} \text{cm}^{-1} \quad (6)$$

the band maximum.

Shortly thereafter, the binuclear mixed-valence complexes **1**, formally containing Ru(II) and Ru(III) (26), and **2**, formally containing Fe(II) and Fe(III) (24), were synthesized and their electronic



1



2

spectra interpreted in light of Hush's models. Discrete, soluble species such as **1** and **2** were seen to provide a particularly powerful probe because, being based on substitution inert metal centers, they can be studied in a variety of media in the confidence that the composition of the metal coordination spheres is retained. As a result of these efforts synthesis and characterization of binuclear mixed-valence complexes were perceived as a means of probing in depth the energetics of solution electron transfer processes and the mechanisms and magnitudes of electronic interactions between metal centers. In the past 12 years more than 100 complexes related to **1** have been synthesized and characterized [a feat, it should be noted, only possible because of the earlier development of viable synthetic methods in the laboratories of Taube (45), Meyer (80), and Malin (131)].

In this article, those most closely related to **1**—M(II)–M(III) bridged complexes based on the d^6 – d^5 metal centers, iron, ruthenium and osmium—are reviewed. The emphasis is on the interrelationships between the physical properties of these complexes and the mechanisms of electron transfer processes. General information concerning the models used to understand the properties of mixed-valence complexes (Section II) and the physical and chemical properties of the related mononuclear complexes (Section III) are first presented as background. The problem of ascertaining the nature of the electronic structure of mixed-valence species is considered in Section IV, while the stabilities of the species are taken up in Section V. In the last section parameters extracted from the spectra of mixed-valence complexes are used to model thermal electron transfer reactions for these and related species.

II. MIXED-VALENCE COMPLEXES AND THE DYNAMICS OF ELECTRON TRANSFER REACTIONS

A. General Considerations

Consider a bridged binuclear metal complex containing a metal center M and its one-electron oxidation product M^+ . In general the bridge (denoted \rightsquigarrow) may range from a long organic bridging group to a single atom (O^{2-}) or nothing (metal–metal bond) and has a great influence on the coupling between the metal centers (14, 30). To illustrate the connection between electron transfer processes (54, 70, 71, 113–5) and mixed-valence compounds (48, 52, 79–82), a binuclear complex is considered in which the distance r between M and M^+ is moderate, the electronic coupling H_{AB} between them is small, and the constituents of the metal coordination spheres are identical. Assume that one of the metal sites is "labeled" so that the

left- and right-hand sites can be distinguished. The energy of the electron (or electron hole) at the two sites is, however, identical since the constituents of the two sites are the same, that is, the equilibrium constant for Eq. 7 is unity ($\Delta G^0 = 0$), and the species on the left- and right-hand sides of Eq. 7 are energetically degenerate electronic isomers.



Isomer $M \rightsquigarrow M^+$ may convert into isomer $M^+ \rightsquigarrow M$ with a first-order rate constant (114, 117)

$$k_{th} = \kappa \nu_n \exp(-\Delta G_{th}^*/RT) \quad (8)$$

where κ is an adiabaticity factor (see below) and ν_n , the nuclear frequency factor, is $(1-10) \times 10^{12} \text{ sec}^{-1}$ at 25°C . Although no net free-energy change accompanies this electron transfer, there is an activation barrier ΔG_{th}^* to the process imposed by the following factors, which are illustrated in Fig. 1. (For simplicity, the ligands are omitted in Fig. 1 and Eq. 7, but the circles in Fig. 1 represent the whole metal-ligand coordination sphere, not just the metal ion.) In general, the metal-ligand bond lengths (d_2^0, d_3^0) and force constants (f_2, f_3) differ for M and M^+ . In addition, if $(M \rightsquigarrow M^+)$ is in solution, the solvation of the two sites also differs. As a consequence of these differing inner-shell and outer-shell environments, the electron transfer, Eq. 7, is accompanied by net nuclear rearrangements. Nuclear motion occurs on a time scale (10^{-13} sec) much longer than electronic motion ($<10^{-15} \text{ sec}$) (this is the Franck-Condon principle); this gives rise to the electron transfer activation barrier. If spontaneous electron transfer were to occur between M and M^+ in their equilibrium configurations (bond length and solvation states), the product would be formed in a vibrationally ex-

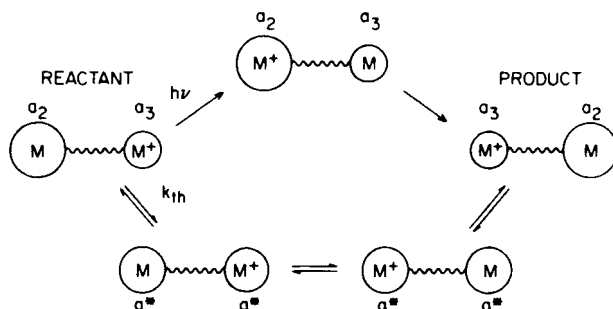


Figure 1. Thermal and optical electron transfer processes in a symmetric binuclear mixed-valence complex.

cited state; M^+ having the metal–ligand bond lengths and solvation of M and M in a configuration appropriate to M^+ would result and energy would not be conserved. This thermally “forbidden” pathway is the upper route shown in Fig. 1. In fact, for the thermal electron transfer, rearrangement of the ligand and solvent nuclei about M and M^+ precedes the electron transfer step with the degree of rearrangement required, constituting an activation barrier to the process. The electron transfer occurs within an activated complex in which the $M-L$ and M^+-L bond lengths d^* , etc., are the same and are intermediate between the equilibrium $M-L$ and M^+-L values d_2^0 and d_3^0 . If the electron transfer occurs with unit probability ($\kappa = 1$) in the activated complex, the reaction is adiabatic; if $\kappa < 1$, the electron transfer is nonadiabatic. This thermally allowed pathway is the lower route shown in Fig. 1.

Although thermal electron transfer does not proceed without prior rearrangement of the inner and outer shells, the upper pathway in Fig. 1 can be induced when the absorption of light of the correct frequency supplies the energy required to form the excited state $^*[M \rightsquigarrow M^+]$. The upper pathway is thus denoted light induced or *optical electron transfer* and occurs when $E_{op} = h\nu$. Such light absorption gives rise to intervalence transfer (IT) absorption (also termed metal-to-metal charge transfer absorption).

The energetic relations between the barriers for thermal and optical electron transfer are related in theory as is shown in Fig. 2, a plot of potential energy versus nuclear configuration. The left-hand parabola is the potential energy surface for $M \rightsquigarrow M^+$ (electron on left-hand side); the right-hand

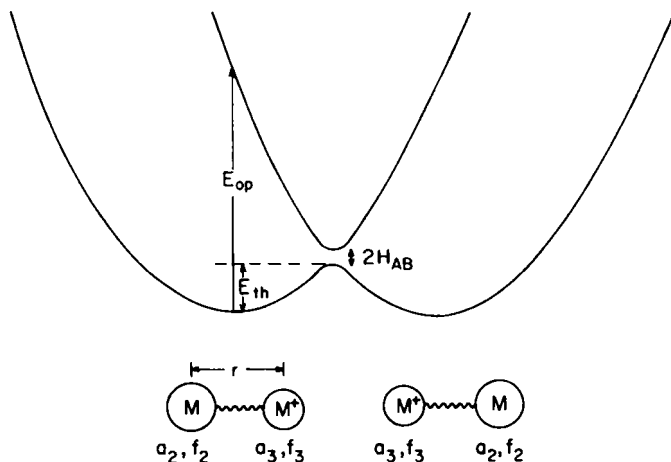


Figure 2. Potential energy versus nuclear configuration for a symmetric mixed-valence complex.

curve is for $M^+ \rightsquigarrow M$ (electron on right-hand side). The minima are displaced along the nuclear configuration coordinate because the nuclear configurations of $M \rightsquigarrow M^+$ and $M^+ \rightsquigarrow M$ differ (at the left, the left-hand site has bond lengths, d_2^0 , etc.; at the right, this site has bond lengths d_3^0 , etc.). The curves split at the intersection by $2H_{AB}$, where H_{AB} is the resonance energy between the two states. In the thermal electron transfer, Eq. 7, the system moves from left to right (horizontally) along the lower surface and (classically) passes over the barrier of height E_{th} . Optical electron transfer takes place when light of the correct energy ($E_{op} = \lambda = h\nu$) is absorbed and the system passes *vertically* from the lower to the upper surface (arrow shown at the left-hand side). Provided that $E_{th} = \Delta G_{th}^*$ and H_{AB} is very small, the barriers to optical and thermal electron transfer are simply related by a factor of four (48, 52), that is

$$E_{op} = \lambda = 4 \Delta G_{th}^* \quad (1)$$

It is thus expected that mixed valence ions such as $M^+ \rightsquigarrow M$ should exhibit absorption bands that occur at $h\nu = \lambda$. The absorption maxima are related to thermal electron transfer barriers for the ions and are a function of the differences in metal-ligand bond lengths ($d_2^0 - d_3^0$), the distance r between the metal centers, the sizes of the metal coordination spheres, and the properties of the solvent and other factors that are discussed later.

B. Classification of Mixed-Valence Complexes

Robin and Day (101) have distinguished three broad classes of mixed-valence materials: In a Class I mixed-valence compound the interaction between M and M^+ centers is so weak (because the $M-M^+$ separation is great, the M and M^+ environments are extremely different or for other reasons) that the mixed-valence material exhibits only the properties observed for isolated mononuclear M and M^+ complexes. In Class III, the opposite extreme is found: Interaction between the two centers is so great that the properties of isolated M and M^+ are absent and only new properties characteristic of the $(M-M)^+$ unit are discerned. Class II materials exhibit slightly perturbed M and M^+ characteristics and may also manifest properties not associated with the isolated units. Equation 1 is applicable when $H_{AB} \approx 0$, that is, the interaction between the two sites is negligible, that is, for a Class I or weakly coupled Class II system. As H_{AB} increases it lowers the thermal electron transfer barrier and $E_{th} = (\lambda/4) - H_{AB}$. When H_{AB} becomes very large, the lower surface no longer features two minima corresponding to localized mixed-valence ions $M \rightsquigarrow M^+$ and $M^+ \rightsquigarrow M$; instead there is a single minimum for the delocalized species $(M \rightsquigarrow M)^+$ (55). This progres-

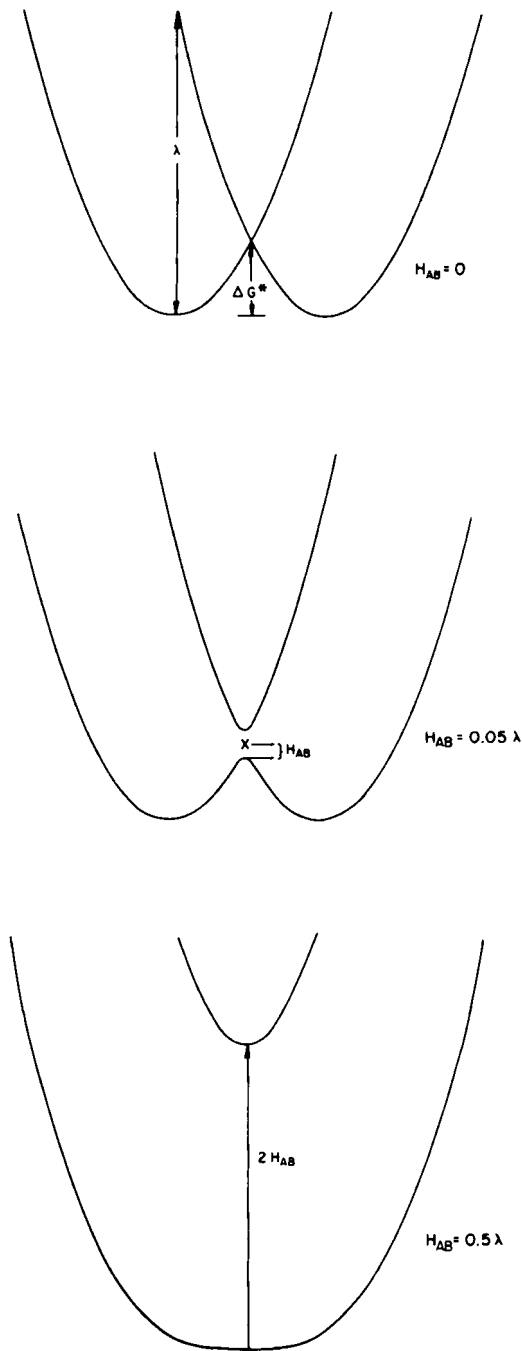


Figure 3. Potential energy versus nuclear configuration for a symmetric mixed-valence complex as a function of λ and H_{AB} .

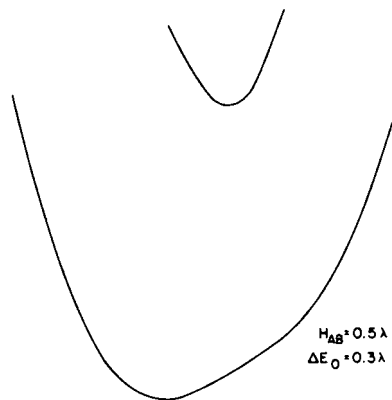
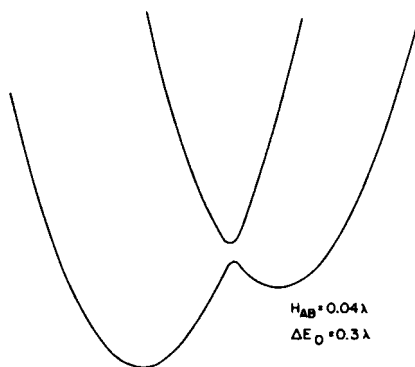
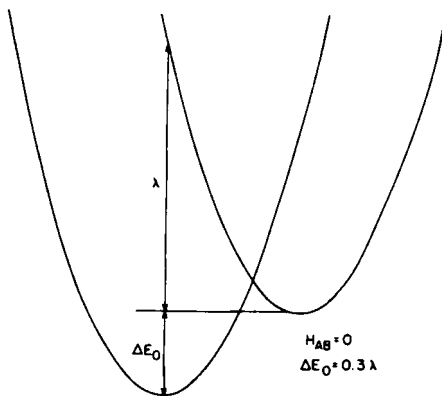


Figure 4. Potential energy versus nuclear configuration for an asymmetric mixed-valence complex as a function of λ and H_{AB} .

sion as H_{AB} increases relative to λ is shown in Fig. 3 in which the top, center, and bottom figures correspond to Class I, II, and III behavior, respectively. The top curves (the "zero-order" surfaces) are for $E_{op} = \lambda$, $H_{AB} = 0$. For such a Class I system the thermal electron transfer process is nonadiabatic; since $H_{AB} = 0$, the system tends *not* to cross from the left-hand to the right-hand curve at the intersection. Furthermore, since the intensity of the intervalence transfer band at $h\nu = \lambda$ depends on H_{AB} , it may not be observed for a Class I species. The center curves are calculated for the same zero-order curves (same λ value as the top), but with $H_{AB} = 0.05\lambda$. The surfaces split by $2H_{AB}$ at the intersection, increasing the probability that the system will remain on the lower surface and that the thermal electron transfer will be adiabatic. IT absorption at $h\nu = \lambda$ is now expected to have measurable intensity because of the magnitude of H_{AB} . If $H_{AB} > \lambda/2$ the lower surface possesses a single minimum as shown at the bottom of Fig. 3. Note that the Class III ion also undergoes light absorption by virtue of its mixed-valence nature—but at $h\nu = 2H_{AB}$. Thus the position of a mixed-valence band of a Class II ion is related to E_{th} , but that for a Class III ion to H_{AB} .

The effects of introducing ΔE_0 , an energetic difference between the two sites is shown in Fig. 4.

C. Analysis of Intervalence Spectra

The most widely used analysis of intervalence spectra is that given originally by Hush and was summarized in Eqs. 1–6. For asymmetric systems for which an energetic difference ΔE_0 between the sites exists, the following additional relations are of value:

$$E_{op} = \lambda + \Delta E_0 = 2(\lambda E_{th})^{1/2} \quad (1a)$$

$$E_{th} = \frac{(\lambda + \Delta E_0)^2}{4\lambda}$$

$$\frac{\bar{\nu}_{max} - (\Delta\bar{\nu}_{1/2})^2}{2310} = \Delta E_0 \text{ cm}^{-1} \quad (2a)$$

[Note that $\Delta\bar{\nu}_{1/2}$ is defined as the value of $\Delta\bar{\nu}$ at which

$$\frac{I_\nu \bar{\nu}_{max}}{I_{max} \bar{\nu}} = \frac{1}{2}$$

but that it is most commonly evaluated as $\Delta\bar{\nu}$ for which $I/I_{max} = \frac{1}{2}$.] The

temperature dependence of the band width is given by

$$E_{op} = (16 \ln 2kT)^{-1} \Delta E_{1/2}^2 + E_0 \quad (9)$$

All of the Hush relationships given here are for the high-temperature (classical) limit. The Hush model is fundamentally a classical (high-temperature) model in which both inner-shell and solvent are treated.

While several treatments emphasizing the inner shell have appeared (13, 64, 75, 76, 94, 95) that presented in 1977 by Piepho, Krausz, and Schatz (PKS) (86) has received the most attention. In this vibronic coupling model for mixed-valence systems, only symmetric inner-shell modes of the couple were treated (the surrounding medium was neglected) (86). The band maximum, intensity, and shape are iteratively fitted to three parameters: a vibronic coupling parameter λ , an electronic coupling parameter ϵ , and $\bar{\nu}$ the wavenumber of the totally symmetric metal-ligand stretching vibration (usually taken as 500 cm^{-1}). In terms of the notation used in this paper, the PKS relations are

$$\bar{\nu} = \frac{1}{c} \sqrt{\frac{f}{4\pi^2\mu}} \text{ cm}^{-1} \quad (10)$$

where c is the speed of light, f is the metal-ligand force constant ($f_2 = f_3 = f$), and μ is the reduced metal-ligand mass.

$$\epsilon\bar{\nu} = H_{AB} \text{ cm}^{-1} \quad (11)$$

and

$$E_{op} = 2\lambda^2\bar{\nu} \text{ cm}^{-1} \quad (12)$$

The treatment has been applied to **1** (86) and several other systems (87, 104, 140, 141); the resonance Raman spectra of mixed valence species have been predicted (142, 143) and far infrared tunneling transitions have been predicted (103) but not observed (60).

Hush has criticized the model for the assumption of a *single* frequency, arguing that when **1** (a delocalized complex) is excited to its upper surface, the average bond lengths of the complex must change and attributes the bandwidth and asymmetry to this effect (56). PKS have criticized Hush for neglecting quantum effects introduced by the high frequency of the inner-shell modes (140, 141).

Recently Buhks (12) criticized the PKS model for its neglect of medium repolarization and has given a rather complex analysis in which both low-

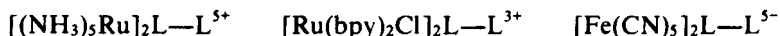
frequency solvent (classical) modes and high-frequency inner-shell modes are treated. For the high-temperature limit and when $H_{AB} \ll E_{out}$, Buhks' linewidth is the same as that given in Eq. 2; the observation of $\Delta\bar{\nu}_{1/2}$ values larger than calculated from Eq. 2 is attributed to the participation of quantum modes (a classical model is valid for the outer-, not the inner-, shell). Buhks has provided model calculations of bandshapes (assumed constant: $E_{in} = 1.0$ kK and $\bar{\nu}_{M-1} = 500$ cm^{-1}) from which E_{out} and H_{AB} for both Class II and III ions may be deduced. Clearly Buhks' calculations are more realistic; they are also more difficult to employ.

Results obtained by the three analyses are given in Table I. Not surprisingly, excellent agreement for H_{AB} ($= J = \epsilon\bar{\nu} = V$) is obtained for the last three complexes in which delocalized systems are involved; the electronic coupling parameter is deduced from $\bar{\nu}_{max}$ in all three treatments.

The model described by Buhks has the virtue of completeness—but is intrinsically rather unwieldy. That proposed by PKS is intuitively appealing, but neglects the medium—which, as is mentioned in the next sections, is the major source of the electron transfer barrier for many of the species treated in this article. Thus the Hush treatment remains the most powerful and tractable for species of this type and is therefore used in the following sections.

III. THE FRAGMENTS: PROPERTIES OF THE MONONUCLEAR SYSTEMS

In this article the properties of mixed-valence complexes derived by varying the structure of a bidentate bridging ligand L—L in structures such as 3–5 and related complexes are discussed. While a number of other



soluble mixed-valence complexes are known [e.g., 2 (24) and its analogues (23, 25), Cu(I)—Cu(II) species (47), and Mn(III)—Mn(IV) (22) species among many others], the work with the d^6-d^5 complexes such as 3–5 has been especially extensive and systematic on account of the substitutional and electron transfer properties of these metal centers (46, 122, 126). Because these properties are most readily illustrated by the properties of mononuclear complexes and because a familiarity with the physical and chemical properties of these "fragments" is useful in understanding the properties of the mixed-valence derivatives, a brief account of the behavior of the monomeric systems is given in this section.

TABLE I
Analyses of Intervals Spectra

Complex	Observed ^a			Calculated (kK)				
	$\bar{\nu}_{\max}$, kK	$10^{-2} \epsilon$, $M^{-1} \text{cm}^{-1}$	$\Delta\bar{\nu}_{1/2}$, kK	χ	J	$2\lambda^2\bar{\nu}$	PKS ^c	Buhks ^d
							$\epsilon\bar{\nu}$	E_{out}
$[\text{Ru}(\text{bpy})_2\text{Cl}]pz^{3+}$ /	7.7	4.5	5	7.7	0.4	9.4	1.3	(-7)
$[\text{Ru}(\text{bpy})_2\text{Cl}]pym^{3+}$ g	7.35	0.4	5.5	7.35	0.1	8.9	0.4	(-6)
$[(\text{NH}_3)_5\text{Ru}]_2(4,4'\text{-bpy})^{5+}$ h	9.71	9.2	5.2	9.71	0.3	11.5	2.5	(-9)
$[(\text{NC})_5\text{Fe}]pz^{3-}$ i	8.3	4.8	22	8.3	0.9	—	—	-8
$[(\text{NH}_3)_5\text{Ru}]_2pz^{3+}$ j	6.37	50	1.4	(3.5) ^f	3.1 ^e	7.3	3.0	4.3
$[(\text{NH}_3)_5\text{Ru}]_2(\text{N}\equiv\text{C}-)_{2}^{3+}$ k	6.99	4.1	1.6	—	3.5	8.4	3.0	5.0
$[(\text{NH}_3)_5\text{Ru}]_2(\text{NC}-\overset{\text{t-Bu}}{\text{C}}-\text{CN})^{4+}$ l	8.55	160	2.2	—	4.3	0.25	4.3	6.5

^aThe first two complexes were studied in acetonitrile solvent; the rest in D_2O .

^b $\chi = E_{\text{op}} = \bar{\nu}_{\max}$, $J = H_{AB}$; see Eq. 6.

^c Adapted from Ref. 121. $2\lambda^2\bar{\nu} = E_{\text{op}} = \bar{\nu}_{\max}$; $\epsilon\bar{\nu} = H_{AB}$, where $\bar{\nu} = 500 \text{ cm}^{-1}$.

^d Adapted from Ref. 12; E_{in} was taken as 1 kK; $V = H_{AB}$, assessed from Eq. 6 for the first four entries.

^e Ref. 56.

^f Refs. 15 and 93.

^g Refs. 91 and 93.

^h Ref. 128.

ⁱ Ref. 43.

^j Ref. 26.

^k Ref. 129.

^l Ref. 61.

In the mononuclear series based on $ML = (NH_3)_5RuL^{n+}$, $Ru(bpy)_2ClL^{n+}$, $Fe(CN)_5L^{n-}$, and $Os(NH_3)_5L^{n+}$, the M(III) complexes are substitution inert, undergoing ligand loss on a time scale of hours [for $Fe(CN)_5L^{n-}$] to days or longer at room temperature. By contrast, substitution is relatively rapid for the M(II) complexes when the sixth ligand is a weak one such as water or acetone. Thus the preparative strategy usually exploited is reaction of $(NH_3)_5RuS^{2+}$ (45, 58, 106), $(bpy)_2ClRuS^+$ (80), or $Fe(CN)_5S^{3-}$ (131) (S a solvent molecule) with excess L to produce the M(II)—L complex. If M(III)—L is desired, it is prepared via oxidation of M(II)—L. With few exceptions the M(II)—L and M(III)—L combinations are resistant to substitution for experimentally convenient periods (hours or longer), so that both are readily amenable to physical and chemical characterization and are useful as synthetic intermediates. [Note, however, that the $Ru(edta)L^{2-}$ and $Ru(edta)L^{3-}$ series are exceptional: Neither oxidation state is especially substitution inert and the Ru(III) complexes are *more* substitution labile than their Ru(II) counterparts (73). In addition the preparative routes presently available for the osmium amines leave much to be desired (69, 105, 123).]

Many facets of the behavior of M(II)—L and M(III)—L are dominated by the fact that M(II) exhibits π -base properties. M(II) is rich in πd (t_{2g} in octahedral symmetry) electron density, which may be delocalized onto the vacant ligand orbitals of π symmetry as is illustrated in Fig. 5. When L is an N-aromatic heterocycle (a moderately strong π acid) intense M(II)—L charge-transfer (MLCT) absorption occurs in the visible spectral region as is shown in Table II. There it is evident that, for the most part, the MLCT absorption maximum shifts to lower energy (longer wavelength) as the reducibility of L (first row) increases, reflecting the fact that the ground states are largely metal centered [M(II)—L], in character, while the excited states are largely ligand centered [M(III)—L⁻] in character. The extent of mixing of the M(II)— πd and L— π^* orbitals is, however, significant—being of the order of ~ 0.05 electron for $(NH_3)_5RuL^{2+}$ (149) and probably comparable for $Fe(CN)_5L^{3-}$ and $Ru(edta)L^{2-}$. For $Ru(bpy)_2ClL^+$ the mixing is likely less

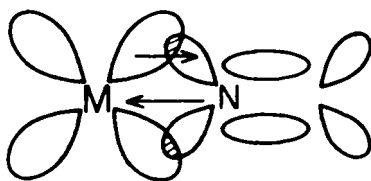
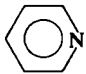
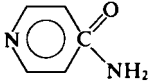

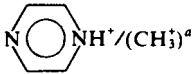
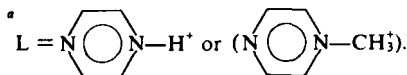


Figure 5. The πd -L- π^* interaction.

TABLE II
Metal-to-Ligand Charge Transfer Absorption Bands (λ_{\max} in nm) for Divalent Complexes in Aqueous Solution

				
$E_{1/2}(L)_V^b$	-2.20	—	-1.57	(-0.19)
$Fe(CN)_5L^{3- c}$	362	434	450	(662)
$Ru(bpy)_2CIL^{+ d}$	500,460 ^e ~385 ^f	—	478,459 ^e ~350 ^e	—
$Ru(NH_3)_5L^{2+ g}$	407	479	472	529 (538)
$Ru(edta)L^{2- h}$	382	460	463	(538)
$Os(NH_3)_5L^{2+ i}$	430	508	460	430



^b Relative to a Hg pool in dimethyl formamide solvent; from Ref. 139.

^c Ref. 131.

^d In CH_3CN solvent; Ref. 15.

^e $d \rightarrow$ bpy charge transfer.

^f $d \rightarrow$ L charge transfer.

^g Refs. 45, 123.

^h Ref. 73.

ⁱ Ref. 105.

since the 2,2'-bpy ligands (also π acids) lower the electron density on the metal center. [Note also that the Ru(II)-to-2,2'-bpy transitions at 450–500 nm, rather than the Ru(II)-to-L MLCT transitions at ~350 nm, dominate the visible spectra of $Ru(bpy)_2CIL^+$.] For $Os(NH_3)_5L^{2+}$, however, this back-bonding interaction is markedly greater as a result of the fact that the Os(II)- d and L- π^* orbitals are of comparable energy (69). The qualitative difference resulting from going from $Ru^{II}(NH_3)_5L$ to $Os^{II}(NH_3)_5L$ is illustrated by the values for LH^+ acidities given in Table III. The affinity of

TABLE III
Effects of Coordination on the Acidity of pzH^+ ^a

Acid	pK_a	Ref.
pzH^+	0.6	45
$Ru(NH_3)_5pzH^{4+}$	-1.0	45
$Ru(NH_3)_5pzH^{3+}$	2.5	45
$Os(NH_3)_5pzH^{3+}$	7.4	105

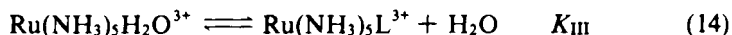
^a Adapted from Ref. 123.

pyrazine for protons is enhanced two orders of magnitude upon binding to $\text{Ru}(\text{NH}_3)_5^{2+}$ (45), but nearly seven orders of magnitude upon binding to $\text{Os}(\text{NH}_3)_5^{2+}$ (105). These effects reflect the accumulation of M(II) electron density on L and LH^+ as the extent of M(II)- d and L- π^* interaction increases.

The M(II) backbonding interaction has a pronounced role in the redox properties of these complexes, as well. As is shown in Table IV, the reducing power of $\text{Ru}(\text{NH}_3)_5\text{L}^{2+}$ decreases as the π acidity of L increases. This has been attributed to the poor π basicity of $\text{Ru}(\text{NH}_3)_5^{3+}$: The affinity of $\text{Ru}(\text{NH}_3)_5^{2+}$ for L increases with the π acidity of L while



that of $\text{Ru}(\text{NH}_3)_5^{3+}$ does not. For L = py, $K_{\text{II}} = 2.4 \times 10^7 M^{-1}$ (106)



[in contrast to that for NH_3 , $K_{\text{II}} = 3.5 \times 10^4 M^{-1}$ (106)], $K_{\text{III}} = 1.5 \times 10^4 M^{-1}$ and $K_{\text{II}}/K_{\text{III}} = 1.6 \times 10^3$ (62, 106), which gives rise to the fact that $\text{Ru}(\text{NH}_3)_5\text{py}^{2+}$ is a poorer reductant than $\text{Ru}(\text{NH}_3)_5\text{H}_2\text{O}^{2+}$. A similar trend is evident for $\text{Fe}(\text{CN})_5\text{L}^{2-/3-}$ and $\text{Os}(\text{NH}_3)_5\text{L}^{3+/2+}$, although the effect is much smaller for the former and much larger for the latter. For $\text{Ru}(\text{edta})\text{L}^{-2-}$, the relatively small E^0 shifts with L (compared with those for $\text{Ru}(\text{NH}_3)_5\text{L}^{3+/2+}$) have been attributed to the ability of the electron-rich Ru(III) in $\text{Ru}(\text{edta})\text{L}^-$

TABLE IV
Reduction Potentials ($E_{1/2}$, V vs SHE) of d^3-d^6 Couples in Aqueous Solution

	H ₂ O	py	pz	N ₂
$\text{Fe}(\text{CN})_5\text{L}^{2-/3-}$ ^a	0.39	0.47	0.55	—
$\text{Ru}(\text{bpy})_2\text{ClL}^{2+/+}$	—	0.79 ^{b,c}	0.88 ^{c,d}	—
$\text{Ru}(\text{NH}_3)_5\text{L}^{3+/2+}$	0.07 ^e	0.30 ^e	0.49 ^f	+1.12 ^g
$\text{Ru}(\text{edta})\text{L}^{-2-}$	-0.01 ^h	+0.10 ^h	+0.24 ^h	—
$\text{Os}(\text{NH}_3)_5\text{L}^{3+/2+}$	-0.73 ⁱ	-0.40 ^j	-0.09 ^j	+0.58 ^j

^aRef. 130.

^bRef. 15.

^c $E_{1/2}$ vs. SSCE in acetonitrile.

^dRef. 17.

^eRef. 72.

^fRef. 67.

^gRef. 42.

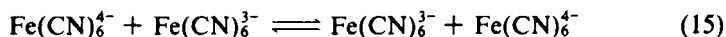
^hRef. 73.

ⁱRef. 51.

^jRef. 10, 105.

to act as a π donor (73) and the relatively long lifetime of $\text{Os}(\text{NH}_3)_5\text{N}_2^{3+}$ suggests moderate π -donor properties for this metal center as well. On the whole, however, the M(III) centers are better regarded as π acceptors (acids) by virtue of their high charge and half vacant π - d acceptor orbital, as is suggested by the observation of low-energy ligand-to-metal charge-transfer (LMCT) bands in the spectra of deprotonated malonodinitrile bridged complexes and other properties of these species (61).

The intrinsic reactivity of a couple with respect to outer-sphere electron transfer processes is reflected in the rate constant for its bimolecular self-exchange reaction, for example,

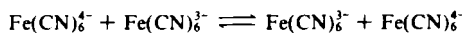


As is shown in Table V the exchange reactions of all the fragments considered here are rapid and ΔG_{th}^* , the activation barrier to outer-sphere electron transfer, is small. The small barriers result, in part, from the electronic properties of the couples: Because the low-spin d^6 - d^5 couples differ by an electron in a nonbonding, rather than an antibonding, orbital only small changes in metal-ligand bond lengths (due predominantly to the changing effective metal center charge) ensue when an electron is lost or gained by the complex. Metal-ligand bond length data as a function of oxidation

TABLE V
Electron Exchange Rate Parameters at $\sim 25^\circ\text{C}^a$

Couple	μ, M^b	$k, M^{-1} \text{sec}^{-1}$	Ref.
$\text{Fe}(\text{CN})_6^{4-/3-}$	$0.1M \text{K}^+$ $\mu \longrightarrow 0$	9.6×10^3 25	18
$\text{Fe}(\text{CN})_5\text{py}^{3-/2-}$	$0.05M \text{K}^+$ $\mu \longrightarrow 0$	7×10^5 2.5×10^6	133
$\text{Ru}(\text{bpy})_2\text{Clpy}^{+/2+}$	$\mu \sim 0^c$	4.9×10^7	15
$\text{Ru}(\text{bpy})_3^{2+/3+}$	1.0	1.2×10^9	147
$\text{Ru}(\text{NH}_3)_6^{2+/3+}$	0.01	4.3×10^3	78
$\text{Ru}(\text{NH}_3)_5\text{py}^{2+/3+}$	0.1	1.1×10^5	9
$\text{Ru}(\text{NH}_3)_4\text{bpy}^{2+/3+}$	0.1	7.7×10^5	7
$\text{Ru}(\text{edta})\text{py}^{2-/}$	0.2	$> 10^4$	73
$\text{Os}(\text{NH}_3)_6^{2+/3+}$	0.5	$\sim 10^3$	31
$\text{Os}(\text{NH}_3)_5\text{N}_2^{2+/3+}$	0.5	$\sim 10^3$	31

^aFor the exchange reactions, for example,



^bIn water as solvent, unless otherwise stated.

^cIn acetonitrile solvent, no added electrolyte.

TABLE VI
 Metal-Ligand Bond Length (d^0) Values for Low Spin d^6 and d^5 Complexes

Complex	Bond	d^0 Å		Ref.
		M(II)—L	M(III)—L	
$\text{Fe}(\text{CN})_6^{4-/3-}$	Fe—C	1.900(7)	1.926(3)	120
$\text{Fe}(\text{phen})_3^{2+/3+}$	Fe—N	1.97(1)	1.973	2,148
$\text{Ru}(\text{NH}_3)_6^{2+/3+}$	Ru—N	2.144(4)	2.104(4)	110
$\text{Ru}(\text{NH}_3)_5\text{pz}^{2+/3+}$	Ru—pz	2.006(6)	2.076(8)	50
<i>cis</i> - $\text{Ru}(\text{NH}_3)_4(\text{isn})_2^{2+/3+}$	Ru—NH ₃	2.155(6)	2.112(7)	96
	Ru— <i>isn</i>	2.060(4)	2.099(4)	
	Ru—NH ₃ <i>ax</i>	2.143(5)	2.125(7)	
$\text{Ru}(\text{bpy})_3^{2+}$	Ru—N	<i>trans</i> 2.170(6)	—	100
		2.056(6)		

state are given in Table VI for some low-spin d^6 - d^5 couples. None of the bond length differences $|d_2^0 - d_3^0|$ exceeds 0.1 Å. (By contrast, note that the bond length differences for couples with much slower exchange rates may be as great as 0.2 Å.) Note also that the M(II)—L bond length may be the same as the M(III)—L bond length [$\text{Fe}(\text{phen})_3^{3+/2+}$] or shorter than the M(III)—L bond length (Fe—CN and Ru—pz). Thus the effects of M(II)—L backbonding may be quite dramatic for some M(II)—L combinations. Additional factors influencing the magnitude of the electron exchange rates are (7, 116, 117): (1) the work required to bring the complexes into close proximity, (2) the outer-shell rearrangement barrier (ΔG_{out}^*), stemming from the fact that the polarization of the solvent surrounding the reactant complexes changes upon electron transfer, and (3) the adiabaticity factor (κ the probability of electron transfer within the activated complex). The first two factors depend upon the sizes and charges of the complexes, as well as on the nature of the solvent; the latter is determined by the magnitude of the electronic mixing between the metal centers in the transition state and so is a function of their separation and their electronic properties. The evidence presently available suggests that the electronic mixing is significant ($\kappa \sim 1$) for low-spin d^6 - d^5 couples by virtue of either direct M(II)—M(III) d - d or M(II) L—L M(III) ligand mediated d - d overlap when L is a π -acceptor ligand (7, 30). In addition, it is recognized that, while the work terms may be substantial for highly charged species such as $\text{Fe}(\text{CN})_6^{4-}$ - $\text{Fe}(\text{CN})_6^{3-}$ (especially at low ionic strength), the major contribution to the electron transfer barrier for the couples in Table V is the outer-shell barrier (7, 30).

In summary, low-spin M(II) and M(III) iron, ruthenium, and osmium metal centers lend themselves to preparation in a wide variety of stable lig-

and combinations by virtue of both their kinetic and equilibrium behavior. The $M(II)L$ properties are often dominated by the π basicity of low-spin d^6 $M(II)$. The $M(II)L$ — $M(III)L$ couples undergo rather facile electron transfer reactions. As will be seen the combination of substitution inertness and high electron transfer reactivity exhibited by this series is exactly that required for the generation of mixed-valence complexes with interesting properties.

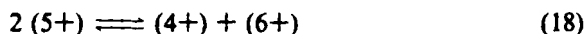
IV. CLASSIFICATION OF MIXED-VALENCE COMPLEXES: CASE HISTORIES FOR $[Ru(NH_3)_5]_2L-L^{5+}$

A. Problems: The Creutz-Taube Ion, $L-L =$ Pyrazine

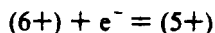
Using methods developed by Ford, Rudd, Gaunder, and Taube (45), **1** was prepared through reaction of $(NH_3)_5RuH_2O^{2+}$ and pyrazine, followed by oxidation of the diruthenium(II) product (26, 27).



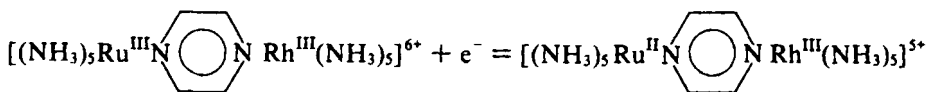
The characterization of **1** in solution was straightforward owing to the great stability of the mixed-valence state ($5+$) with respect to the dimers containing only $Ru(II)$ ($4+$) and only $Ru(III)$ ($6+$), that is, for



the equilibrium constant for disproportionation is $<10^{-6}$. The visible and ultraviolet spectra of **1** revealed only features expected for a species containing $Ru(II)$ and $Ru(III)$ centers, with the visible region being dominated by the metal-to-ligand (pyrazine) charge-transfer band at 565 nm. The reduction potential of the couple

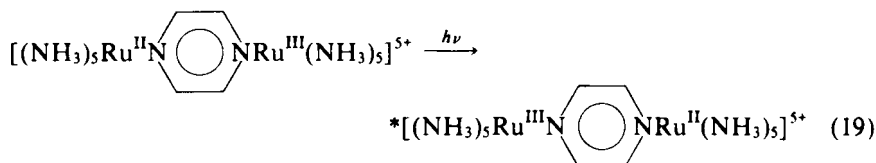


(+0.76 V) was quite similar to that (+0.71 V) for the couple



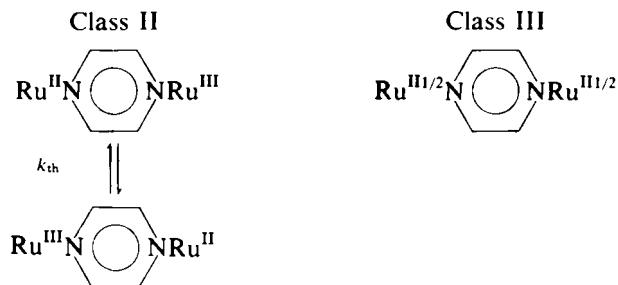
Since Rh(III) is difficult to oxidize or reduce, electron delocalization (H_{AB}) in the mixed-metal dimer should be extremely small. The fact that the two reduction potentials are so similar provided greater weight to the case that **1** is valence trapped (Class II), that is, the electronic structure is better described as $\text{Ru}^{\text{II}}\text{N} \text{---} \text{NRu}^{\text{III}}$ than as $\text{Ru}^{\text{III}/2}\text{N} \text{---} \text{NRu}^{\text{III}/2}$. Since Hush's

theoretical treatment of the relationship between optical and thermal electron transfer had recently appeared, the mixed-valence transition (Eq. 19 where the asterisk denotes a vibrationally excited state) expected in the spectrum of **1** was sought.



The expected new absorption feature was finally discovered in the near-infrared region; a relatively intense ($\epsilon 5.5 \times 10^3 M^{-1} \text{ cm}^{-1}$), asymmetric band, absent in the spectra of the 4+ and 6+ dimers, was found at 1570 nm and assigned to the optical electron transfer transition of a Class II ion. The value of E_{th} (4.5 kcal mole⁻¹) calculated from Eq. 1 seemed reasonable, yielding an estimate of k_{th} for Eq. 1 of $\sim 3 \times 10^9 \text{ sec}^{-1}$. The band position did not, however, shift with the solvent function ($1/D_{\text{op}} - 1/D_{\text{s}}$) as predicted from Eq. 5; in addition the band width at half-height $\Delta\bar{\nu}_{1/2}$ ($1.2 \times 10^3 \text{ cm}^{-1}$) was much smaller than that predicted ($3.8 \times 10^3 \text{ cm}^{-1}$) from Eq. 2. At the time, these inconsistencies were regarded as failures of the model (which had not been widely tested previous to this work), but later many mixed-valence species whose properties were in accord with the Hush model were characterized.

In the 12 years since the synthesis of **1** was reported, at least as many physical techniques have been applied in an effort to determine the nature of the ion—the alternative electronic structures being



A partial summary of the techniques applied is given in Table VII, which is adapted from Table 1 of Ref. 11; a few of the results obtained are discussed here. Since electron transfer is expected to be rapid ($k_{th} > 10^9 \text{ sec}^{-1}$, Eq. 7), even in the case of Class II behavior only techniques with high time resolution might be expected to yield valid results. Thus early NMR studies that gave $k_{th} > 10^7 \text{ sec}^{-1}$ were not especially revealing (41). Ruthenium Mössbauer measurements made on p-toluenesulfonate salts at 4K and interpreted in terms of Class II behavior were unfortunately subject to very large errors (28). ESCA spectra exhibited the features [one $3d_{3/2}$ Ru(II) peak and $3d_{3/2}$ and $3d_{5/2}$ Ru(III) peaks] expected for a Class II ion (21); but this behavior was later shown to be compatible with that of a Class III ion as well (4, 55). The resonance Raman spectrum of **1** is very similar to that of the fully reduced ion; with the exception of a band at 1070 cm^{-1} [which was attributed to pyrazine bound to Ru(III)], a one-to-one correspondence of resonance enhanced bands in the [4+] and [5+] spectra was found and a Class II description was, it was concluded, reasonable (109). Powder EPR results (11) implicating a localized electronic structure were later contradicted by single crystal studies (57) consistent with valence delocalization. A recent crystal structure of a mixed halide salt of **1** gave results consistent with either description (5).

This cursory survey shows that with even the most sophisticated techniques presently available, it can be difficult (or impossible) to distinguish between the localized and delocalized electronic structures of a mixed-valence species such as **1** in which electron exchange is surely $>10^9 \text{ sec}^{-1}$. In retrospect, from at least the standpoint of the nature of **1** in solution, the early near-infrared spectral studies of **1** and the 4,4'-bpy bridged complex **6** (next section), taken with the solvent independent behavior of unambiguously delocalized species, are the most revealing (125). The solvent dependence of the near-infrared band of **6** (and other mixed-valence complexes) has established the applicability of the Hush treatment to species with localized electronic structures. The fact that this solvent dependence is not observed for **1** shows that, at least on the solvent time scale ($>10^{-11} \text{ sec}$ for water), discrete Ru(II) and Ru(III) centers do not exist in **1**. One can imagine that discrete valences exist on a vibrational time scale (125) ($10^{11} \text{ sec}^{-1} < k_{th} < 10^{13} \text{ sec}^{-1}$), that is, that the Ru—N bond lengths differ at the two sites, but infrared measurements in which all detectable metal–ligand vibrational frequencies were found to be averaged (4, 27) indicate that, at least in the solid state, this is not the case. The frequencies do not, however appear averaged in the resonance Raman spectrum (109). Recently, analysis of the shape of the NIR band of **1** has been pursued in an effort to elucidate a detailed description of the ground and excited state potential energy surfaces (4, 55, 56, 86, 104, 140, 141). The analyses have led to the conclusion that **1** is delocalized with $H_{AB} \sim 3.3 \times 10^3 \text{ cm}^{-1}$ (9.2 kcal mole $^{-1}$). Es-

TABLE VII
The Classification of the Electronic Structure of $[(\text{NH}_3)_5\text{Ru}]_2\text{pz}^{2+}$

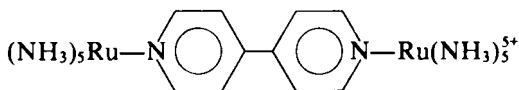
Experiment	Conditions	Time resolution, sec	Year	Conclusion	Ref.
NIR band	20°C, solutions	10^{-11}	1969	localized	26
solvent dependence	80-300K	10^{-6}	1972	delocalized	125
Proton NMR	4K, solid	10^{-9}	1973	delocalized	11, 41
Ru Mössbauer	25°C, KBr	10^{-13}	1976	localized	28
IR: single	pellet		1978	delocalized	4, 27
ν_{NH} , $\nu_{\text{M-N}}$				challenged (lattice effects)	11
ESCA, two	25°C, Ts^a	10^{-17}	1973	localized	21
Ru $3d_{5/2}$ peaks	salt		1976	delocalized	4, 55
Resonance Raman	25°C, solution	10^{-13}	1976	localized	109
Substitution kinetics	25°C, solution	—	1978	not strongly delocalized	125
Reduction potentials	25°C, solution	—	1978	not strongly delocalized	27, 125
EPR spectra	8-50K, powder crystal	10^{-9}	1978	delocalized	11
			1980	localized	57
				delocalized	

^aTs, *p*-toluenesulfonate.

timates of λ for the zero-order surfaces (top of Fig. 3) range from 4.0×10^3 to $7.3 \times 10^3 \text{ cm}^{-1}$. Molecular orbital treatments of the complex as a Class III ion (56, 64, 94, 95) have also appeared.

B. Success of the Hush Model: L—L = 4,4'-bpy

The 4,4'-bipyridine (4,4'-bpy) bridged complex (44, 118, 128) was



6

prepared, in the same way as **1**, by oxidation of the analogous ruthenium(II) dimer, is similar to **1** in that it is purple (λ_{max} 525 nm), and manifests a transition unique to the mixed-valence state in the near-infrared region (λ_{max} 1050 nm in D_2O as solvent). It is however less stable with respect to disproportionation, with K_d for Eq. 18 being 0.04 (118). The NIR spectra of **1** and **6** are compared in Fig. 6. The near-infrared band is broader for **6**; in fact the width in D_2O is somewhat greater than calculated from Eq. 2. Most importantly, the band maximum is solvent dependent. In Fig. 7 the solvent dependences for **1** and **6** are contrasted. From Eqs. 3–5 it is evident that, for small H_{AB} , the slope of the plot is related to the sizes of the ruthenium

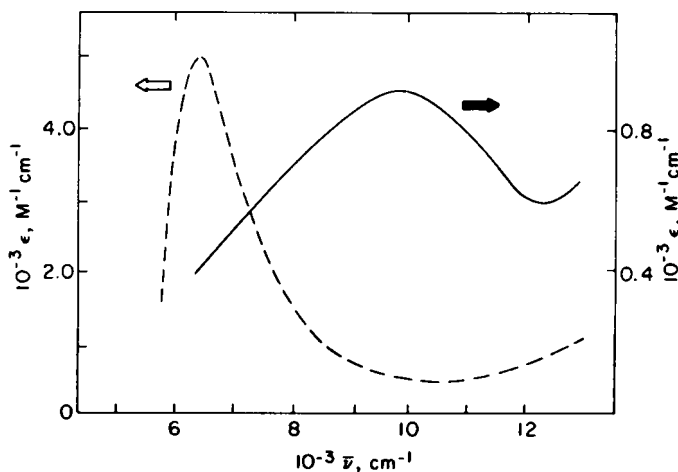


Figure 6. The near-infrared spectra of the pyrazine-bridged complex **1** (broken line, left-hand scale) and the 4,4'-bipyridine-bridged complex **6** (solid line, right-hand scale) in D_2O .

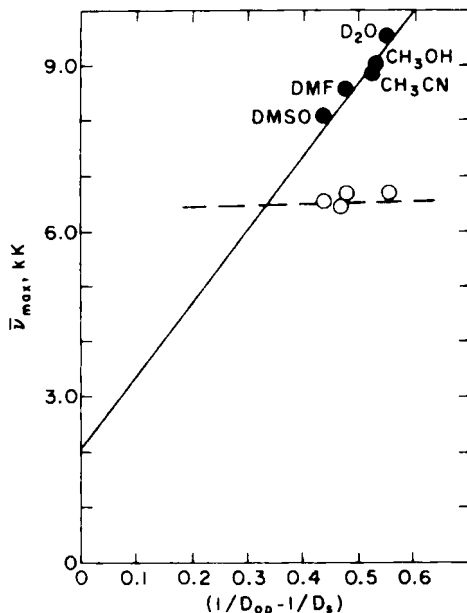


Figure 7. The solvent dependence of the near-infrared band maximum ν_{max} (see Eq. 5). The solid line is for **6** (4,4'-bpy bridge) and the broken line is for **1** (pz bridge).

coordination spheres and the distance between them, while the intercept is related (29) to E_{in} , the inner-shell electron transfer barrier, Eq. 4. The magnitude of H_{AB} is estimated as 400 cm^{-1} ($1.1 \text{ kcal mole}^{-1}$) from Eq. 5. The intercept 2000 cm^{-1} ($5.7 \text{ kcal mole}^{-1}$) obtained for **6** in Fig. 7 may be compared with that calculated (29), $E_{in} = 1400 \text{ cm}^{-1}$ ($4.0 \text{ kcal mole}^{-1}$), from Eq. 4 using metal-ligand bond lengths (50) measured for the mononuclear species $\text{Ru}(\text{NH}_3)_5\text{pz}^{2+}$ and $\text{Ru}(\text{NH}_3)_5\text{pz}^{3+}$ (given in Table VI) and force constants obtained for the $[\text{Ru}(\text{NH}_3)_5]_2\text{pz}^{4+}$ and $\text{Ru}(\text{NH}_3)_5]_2\text{pz}^{6+}$ complexes (109). From the intercept and the magnitude of E_{op} in water, E_{out} for this solvent is 1880 cm^{-1} ($5.4 \text{ kcal mole}^{-1}$). This may be compared with that calculated (29), 1940 cm^{-1} ($5.6 \text{ kcal mole}^{-1}$), from a form of Eq. 5 modified to take into account the fact that the metal coordination spheres in **6** are not spherical (7) (but see Section VI.B). It is clear that the behavior of the mixed-valence band of **6** is semiquantitatively that expected for the optical electron transfer transition of a Class II ion in the Hush model. The magnitude $5.6 \text{ kcal mole}^{-1}$ calculated for ΔG^* in water at 25°C gives $k_{th} \sim 5 \times 10^8 \text{ sec}^{-1}$. Thus, thermal electron transfer between the two sites in this ion occurs on the time scale of $<10^{-8} \text{ sec}$.